Copyright © 2003 Tech Science Press CMES, vol.4, no.1, pp.161-175, 2003

# Elastostatic Deformations of a Thick Plate by using a Higher-Order Shear and Normal Deformable Plate Theory and two Meshless Local Petrov-Galerkin (MLPG) Methods

**L. F. Qian[1,3], R. C. Batra[2] and L. M. Chen[3]**

**Abstract:** We use two meshless local Petrov-Galerkin formulations, namely, the MLPG1 and the MLPG5, to analyze infinitesimal deformations of a homogeneous and isotropic thick elastic plate with a higher-order shear and normal deformable plate theory. It is found that the two MLPG formulations give results very close to those obtained by other researchers and also by the three-dimensional analysis of the problem by the finite element method.

## 1 Introduction

Conventional numerical methods such as the finite element method (FEM), the finite difference method, and the boundary element method have been used to find an approximate solution of an initial-boundary-value problem. More recently, the meshless method has attracted considerable attention due to the flexibility of placing nodes in the domain of study and not needing to connect them into closed polygons. Atluri and Zhu (1998) developed the Meshless Local Petrov-Galerkin (MLPG) method that does not require a background mesh to numerically evaluate integrals appearing in the local weak formulation of the problem. Even though the Galerkin approximation of the problem is obtained when one of the basis functions is taken as the weight function (e.g. see Atluri et al. (1999)), it may not be an optimum choice. By repeated use of the divergence theorem, some or all spatial derivatives on the trial solution can be transferred to the test function. For problems governed by second-order differential equations, Atluri and Shen (2002a,b) have discussed six different choices of test functions and numbered the corresponding formulations as MLPG1, MLPG2,..., MLPG6. Of these, MLPG1, MLPG2 and MLPG6 involve spatial derivatives of the trial solution and the test function of the same order; MLPG6 is the meshless local Galerkin approximation. As also suggested by Atluri and Shen (2002a,b), the MLPG6 required considerably more computer time in accurately evaluating the domain integrals as compared to that for the MLPG1 and the MLPG5 formulations. For the same locations of nodes, computed results were found to be sensitive to the number of Gauss points used. Accordingly, we describe here the MLPG1 and the MLPG5 formulations for the analysis of elastostatic deformations of a thick elastic plate with a higher-order shear and normal deformable plate theory (HOSNDPT) proposed by Batra and Vidoli (2002). Whereas in the MLPG1 the test function equals the weight function of the moving least squares approximation (Lancaster and Silkauskas (1981)), in the MLPG5 the test function equals the Heaviside step function. For problems governed by the Poisson equation, Atluri and Shen (2002a,b) have shown that it is more economical to use the MLPG5 than the Galerkin FEM. The MLPG5 formulation for the HOSNDPT differs from that for the 2-dimensional elastostatic problems in that area integrals do not indentically vanish.

Other recent developments in the MLPG method include the following. Atluri and Zhu (2000) solved elastostatic problems, Lin and Atluri (2000) introduced the upwinding scheme to analyze steady state convection-diffusion problems, and Ching and Batra (2001) used monomials and singular fields near a crack tip to find basis functions by the moving least squares approximation. Gu and Liu (2001) and Batra and Ching (2002) used the Newmark family of methods to analyze 2-dimensional transient elastodynamic problems. The bending of a thin plate has been studied by Long and Atluri (2002), and Warlock et al. (2002) scrutinized elastostatic deforma-

[1] Presently visiting scholar at Virginia Polytechnic Institute and State University

[2] Department of Engineering Science and Mechanics, M/C 0219 Virginia Polytechnic Institute and State University, Blacksburg, Virginia 24061, USA

[3] Nanjing University of Science and Technology, Nanjing 210094, P.R. China

tions of a material compressed in a rough rectangular cavity.

The paper is organized as follows. Sections 2 and 3 briefly review the compatible HOSNDPT and the MLPG formulations respectively. Section 3 also discusses the basis functions and how we impose essential boundary conditions. Numerical examples and comparison of presently computed results with those available in the literature are given in Section 4. Conclusions are summarized in section 5.

## 2 Higher-Order Shear and Normal Deformable Plate Theory

By using a mixed variational principle due to Yang and Batra (1995), Vidoli and Batra (2000) and Batra and Vidoli (2002) derived a first-order and a higher-order theory for thick piezoelectric plates. Salient features of the theory include the satisfaction of natural boundary conditions prescribed on the top and the bottom surfaces of the plate, accounting for both transverse normal and transverse shear deformations, and computations of the transverse normal and the transverse shear stresses from the plate equations rather than by integration through the thickness of the balance of linear momentum. For thick plates, the theory predicts boundary layers near the clamped and the free edges, and the asymmetry in the deformations about the midsurface of a homogeneous thick plate with surface tractions prescribed only on one of the major surfaces. Subsequently, Batra, Vidoli and Vestroni (2002) used the mechanical counterpart of this theory to study the propagation of plane waves and free vibrations of a thick plate. When using the Hellinger-Reissner variational principle, they postulated independent through-the-thickness expansions for displacements and stresses and called it a mixed HOSNDPT. However, when stresses are derived by substituting expansions for displacements in Hooke's law, they called the theory as compatible HOSNDPT. For the same order of expansion of displacements, the mixed HOSNDPT gives through-the-thickness distributions of the transverse normal stress and the transverse shear stress closer to their analytical values than those given by the compatible HOSNDPT. Because of ease of use we employ the latter to analyze static deformations of a thick isotropic and homogeneous linear elastic rectangular plate with different boundary conditions prescribed on the edges. We note that the emphasis here is on the use of the two MLPG formulations for analyzing deformations of a thick plate.

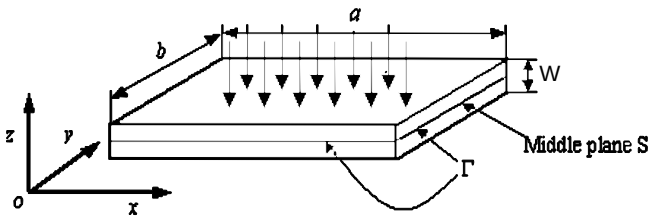


Figure 1: Schematic sketch of the problem

We use rectangular Cartesian coordinates shown in Fig. 1 to describe infinitesimal deformations of a rectangular plate occupying, in the unstressed reference configuration, the region $\Omega$ defined by $0 \le x \le a,\ 0 \le y \le b$ and $-t/2 \le z \le t/2$. The midsurface of the plate is denoted by $S$, and displacements of a point along the $x,\ y$ and $z$ axes by $u,\ v$ and $w$ respectively. For through-the-thickness expansion of displacements, we take for basis functions the Legendre polynomials $L_0(z), L_1(z), L_2(z)\ldots$ normalized by

$$\int_{-t/2}^{t/2} L_i(z)L_j(z)dz = \delta_{ij},\ i,j = 0,1,2,\ldots, \tag{1}$$

where $\delta_{ij}$ is the Kronecker delta. Thus

$$\begin{aligned}
L_0(z) &= \frac{1}{\sqrt{t}}, \quad L_1(z) = 2\sqrt{\frac{3}{t}}\frac{z}{t},\\
L_2(z) &= \frac{1}{2}\sqrt{\frac{5}{t}}\left[12\left(\frac{z}{t}\right)^2 - 1\right],\\
L_3(z) &= \sqrt{\frac{7}{t}}\left[-3\left(\frac{z}{t}\right) + 20\left(\frac{z}{t}\right)^3\right],\\
L_4(z) &= \frac{3}{\sqrt{t}}\left[\frac{3}{8} - 15\left(\frac{z}{t}\right)^2 + 70\left(\frac{z}{t}\right)^4\right],\\
L_5(z) &= \sqrt{\frac{11}{t}}\left[\frac{15}{4}\left(\frac{z}{t}\right) - 70\left(\frac{z}{t}\right)^3 + 252\left(\frac{z}{t}\right)^5\right],\\
L_6(z) &= \sqrt{\frac{13}{t}}\left[-\frac{5}{16} + \frac{105}{4}\left(\frac{z}{t}\right)^2 - 315\left(\frac{z}{t}\right)^4 + 924\left(\frac{z}{t}\right)^6\right],\\
L_7(z) &= \sqrt{\frac{15}{t}}\Big[-\frac{35}{8}\left(\frac{z}{t}\right) + \frac{315}{2}\left(\frac{z}{t}\right)^3\\
&\qquad - 1386\left(\frac{z}{t}\right)^5 + 3432\left(\frac{z}{t}\right)^7\Big], \ldots.
\end{aligned} \tag{2}$$

Following Mindlin and Medick (1959) who attributed it to W. Prager, Batra and Vidoli (2002) set

$$\mathbf{u} = \begin{Bmatrix} u(x,y,z) \\ v(x,y,z) \\ w(x,y,z) \end{Bmatrix} = \sum_{i=0}^{K} \begin{Bmatrix} u_i(x,y) \\ v_i(x,y) \\ w_i(x,y) \end{Bmatrix} L_i(z), \tag{3}$$

for a $K$th order plate theory. When $K \geq 2$, the plate theory is called higher-order. Since we account for both transverse normal and transverse shear deformations, we call it a higher-order shear and normal deformable plate theory (HOSNDPT). Note that $u_i$, $v_i$, $w_i$ $(i = 0,1,2,\ldots,K)$ have the same dimensions. Recalling that $L_i'(z) = dL_i/dz$ is a polynomial of degree $(i-1)$ in $z$, we write

$$L_i'(z) = \sum_{j=0}^{K} d_{ij} L_j(z), \tag{4}$$

where $d_{ij}$ are constants. For $K = 7$,

$$d_{ij} = \frac{2}{t}\begin{bmatrix} 0 & 0 & 0 & 0 & 0 & 0 & 0 & 0 \\ \sqrt{3} & 0 & 0 & 0 & 0 & 0 & 0 & 0 \\ 0 & \sqrt{15} & 0 & 0 & 0 & 0 & 0 & 0 \\ \sqrt{7} & 0 & \sqrt{35} & 0 & 0 & 0 & 0 & 0 \\ 0 & 3\sqrt{3} & 0 & 3\sqrt{7} & 0 & 0 & 0 & 0 \\ \sqrt{11} & 0 & \sqrt{55} & 0 & 3\sqrt{11} & 0 & 0 & 0 \\ 0 & \sqrt{39} & 0 & \sqrt{91} & 0 & \sqrt{143} & 0 & 0 \\ \sqrt{15} & 0 & 5\sqrt{3} & 0 & 3\sqrt{15} & 0 & \sqrt{195} & 0 \end{bmatrix} \tag{5}$$

Note that elements of the first row and the last column of the $(K+1)\times(K+1)$ matrix $d_{ij}$ are zeroes. For infinitesimal deformations, strains $\varepsilon$ are given by

$$\varepsilon = \begin{Bmatrix} \varepsilon_{xx} \\ \varepsilon_{yy} \\ \varepsilon_{zz} \\ 2\varepsilon_{yz} \\ 2\varepsilon_{zx} \\ 2\varepsilon_{xy} \end{Bmatrix} = \sum_{i=0}^{K} \begin{Bmatrix} \dfrac{\partial u_i(x,y)}{\partial x} \\ \dfrac{\partial v_i(x,y)}{\partial y} \\ \displaystyle\sum_{j=0}^{K} w_j(x,y) d_{ji} \\ \dfrac{\partial w_i(x,y)}{\partial y} + \displaystyle\sum_{j=0}^{K} v_j(x,y) d_{ji} \\ \dfrac{\partial w_i(x,y)}{\partial x} + \displaystyle\sum_{j=0}^{K} u_j(x,y) d_{ji} \\ \dfrac{\partial v_i(x,y)}{\partial x} + \dfrac{\partial u_i(x,y)}{\partial y} \end{Bmatrix} L_i(z)$$

$$\equiv \sum_{i=0}^{K} \{\eta_i\} L_i(z), \tag{6}$$

where for $i = 0,1,2,\ldots,K$, $\eta_i$ is a 6-dimensional vector with components

$$\begin{aligned} &\eta_{i(1)} = \partial u_i/\partial x,\ \eta_{i(2)} = \partial v_i/\partial y,\ \eta_{i(3)} = \sum_{j=0}^{K} d_{ji} w_j, \\ &\eta_{i(4)} = \partial w_i/\partial y + \sum_{j=0}^{K} v_j d_{ji},\ \eta_{i(5)} = \partial w_i/\partial x + \sum_{j=0}^{K} u_j d_{ji}, \\ &\eta_{i(6)} = \partial v_i/\partial x + \partial u_i/\partial y. \end{aligned} \tag{7}$$

The terms with $d_{ji}$ couple displacements of the $K$th order with those of the lower order. Using Hooke's law, stresses at a material point $\mathbf{x} = (x,y,z)$ are given by

$$\sigma = \{\sigma_{xx}\ \ \sigma_{yy}\ \ \sigma_{zz}\ \ \sigma_{yz}\ \ \sigma_{zx}\ \ \sigma_{xy}\}^T = \mathbf{D}\varepsilon, \tag{8}$$

where $\mathbf{D}$ is the matrix of elastic constants. Substitution from (6) and (7) into (8) gives stresses at a point $(x,y,z)$ in terms of the displacements and in-plane gradients of displacements of the point $(x,y,0)$.

Let $\tilde{u}$, $\tilde{v}$ and $\tilde{w}$ be three linearly independent functions defined on $\Omega$. Multiplying equations expressing the balance of linear momentum in the $x$, $y$ and $z$ directions by $\tilde{u}$, $\tilde{v}$ and $\tilde{w}$ respectively, adding the three resulting equations, and using the divergence theorem, we obtain

$$\int_\Omega \tilde{\varepsilon}^T \sigma d\Omega - \int_{\partial\Omega} \tilde{\mathbf{u}}^T \sigma \mathbf{n} dS - \int_\Omega \tilde{\mathbf{u}}^T \mathbf{f} d\Omega = 0 \tag{9}$$

where $\mathbf{n}$ is an outward unit normal on $\partial\Omega$, $\mathbf{f}$ is the body force per unit volume, $\tilde{\varepsilon}$ is the 6-dimensional strain vector derived from displacements $\tilde{\mathbf{u}} = (\tilde{u},\tilde{v},\tilde{w})$, and $\partial\Omega$ is the boundary of $\Omega$. Substitution from (6) and (8) into (9) and integration with respect to $z$ from $-t/2$ to $t/2$ gives

$$\begin{aligned} \sum_{i=0}^{K} \Big[ &\int_S \{\tilde{\eta}_i\}^T [D] \{\eta_i\} dS - \int_{\Gamma_u} \{\tilde{u}_i\}^T [n][D]\{\eta_i\} d\Gamma \\ &- \int_{\Gamma_q} \{\tilde{u}_i\}^T \{\overline{q}_i\} d\Gamma - \int_S \{\tilde{u}_i\}^T \{\overline{f}_i\} dS \\ &- L_i(\pm t/2) \int_S \{\tilde{u}_i\}^T \{q^{\pm}\} dS \Big] = 0, \end{aligned} \tag{10}$$

where

$$\{\overline{q}_i\} = \int_{-t/2}^{t/2} L_i(z)\{q\} dz,\ \{\overline{f}_i\} = \int_{-t/2}^{t/2} L_i(z)\{f\} dz, \tag{11}$$

and $\{q^{\pm}\}$ is the traction on the top and the bottom surfaces of the plate. Furthermore, $\Gamma_u$ and $\Gamma_q$ are disjoint

parts of the boundary $\Gamma$ of $S$ where displacements and surface tractions are prescribed respectively as $\{\overline{u}_i\}$ and $\{\overline{q}_i\}$. Usually $\{\tilde{u}_i\}$ is taken to vanish on $\Gamma_u$. However, in the MLPG formulations, it is not necessary to do so since the essential boundary conditions are imposed either by the penalty method or by the elimination of the corresponding degrees of freedom. Here, we have skipped the derivation of plate equations in terms of moments and membrane forces; these are given in Batra and Vidoli (2002) and Batra, Vidoli and Vestroni (2002).

## 3 Implementation of the MLPG Method

### *3.1 Derivation of algebraic equations*

Let $S_\alpha \subset S$ be a smooth 2-dimensional region associated with a node in $S$, $\Gamma_{\alpha u} = \partial S_\alpha \cap \Gamma_u$, $\Gamma_{\alpha q} = \partial S_\alpha \cap \Gamma_q$, $\Gamma_{\alpha 0} = \partial S_\alpha - \Gamma_{\alpha u} - \Gamma_{\alpha q}$, and $\bigcup_{\alpha=1}^{M} S_\alpha = S$; thus $M$ equals the number of nodes in $S$. $S_1, S_2, \ldots, S_M$ need not be of the same shape and size. Let $\phi_1, \phi_2, \ldots, \phi_N$ and $\psi_1, \psi_2, \ldots, \psi_N$ be linearly independent functions defined on $S_\alpha$. For a $K$th order plate theory, there are $3(K+1)$ unknowns $\mathbf{u}_0, \mathbf{u}_1, \ldots, \mathbf{u}_K$ at a point in $S_\alpha$ or $S$. We write these as a $3(K+1)$ dimensional array $\{u\}$, and set

$$\{u(x,y)\} = \sum_{J=1}^{N} [\phi_J(x,y)]\{\delta_J\}, \tag{12}$$

$$\{\tilde{u}(x,y)\} = \sum_{J=1}^{N} [\psi_J(x,y)]\{\tilde{\delta}_J\}, \tag{13}$$

where, for each value of $J$, $\{\delta_J\}$ is a $3(K+1)$ dimensional array and $[\phi_J]$ is a square matrix of $3(K+1)$ rows and columns. Similar remarks apply to $\{\tilde{u}\}$, $[\psi_J]$ and $\{\tilde{\delta}_J\}$. The $3(K+1)$ rows of the matrix $[\phi_J]$ are obtained by repeating $(K+1)$ times the three rows of the $i$th-block given below.

[3 rows of the $i$th block of $\phi_J$] =

$$\left[\begin{array}{ccc|c|ccc|c|ccc} \overbrace{} & & & & \overbrace{} & & & & \overbrace{} & & \\ & & & & & & & & & & \\ 0 & 0 & 0 & \ldots & \phi_J & 0 & 0 & \ldots & 0 & 0 & 0 \\ 0 & 0 & 0 & \ldots & 0 & \phi_J & 0 & \ldots & 0 & 0 & 0 \\ 0 & 0 & 0 & \ldots & 0 & 0 & \phi_J & \ldots & 0 & 0 & 0 \end{array}\right], \tag{14}$$

(with $0$ over the first block, $i$ over the $i$th block, $K$ over the last block)

The functions $\phi_J$ are determined by the moving least squares method described below after eqn. (19). The analogue of unknowns $\{\delta_J\}$ is the nodal displacements in the FEM. However, in the MLPG method, $\{\delta_J\}$ do not generally equal nodal displacements. Substitution from (12) into (7) gives

$$\{\eta\} = \sum_{J=1}^{N} [B_J]\{\delta_J\},\ \{\tilde{\eta}\} = \sum_{J=1}^{N} [\tilde{B}_J]\{\tilde{\delta}_J\}, \tag{15}$$

where $\{\eta\}$ is a $6(K+1)$ dimensional array, and for each value of $J$, $B_J$ is a $6(K+1)\times 3(K+1)$ matrix. The $6(K+1)$ rows of the matrix $B_J$ can be divided into $(K+1)$ blocks of 6 rows each; 6 rows of the $i$th block are given below.

[6 rows of the $i$th block of $B_J$] =

$$\left[\begin{array}{ccc|c|ccc|c|ccc} \overbrace{} & & & & \overbrace{} & & & & \overbrace{} & & \\ & & & & & & & & & & \\ 0 & 0 & 0 & \ldots & \partial\phi_J/\partial x & 0 & 0 & \ldots & 0 & 0 & 0 \\ 0 & 0 & 0 & \ldots & 0 & \partial\phi_J/\partial y & 0 & \ldots & 0 & 0 & 0 \\ 0 & 0 & \phi_J d_{0i} & \ldots & 0 & 0 & \phi_J d_{ii} & \ldots & 0 & 0 & 0 \\ 0 & \phi_J d_{0i} & 0 & \ldots & 0 & \phi_J d_{ii} & \partial\phi_J/\partial y & \ldots & 0 & 0 & 0 \\ \phi_J d_{0i} & 0 & 0 & \ldots & \phi_J d_{ii} & 0 & \partial\phi_J/\partial x & \ldots & 0 & 0 & 0 \\ 0 & 0 & 0 & \ldots & \partial\phi_J/\partial y & \partial\phi_J/\partial x & 0 & \ldots & 0 & 0 & 0 \end{array}\right], \tag{16}$$

(with $0$ over the first block, $i$ over the $i$th block, $K$ over the last block)

and $\tilde{B}_J$ is obtained from $B_J$ by substituting $\psi_J$ for $\phi_J$. The repeated index $i$ on $d_{ii}$ is not summed.

Replacing the domain $S$ of integration in eqn. (10) by $S_\alpha$, substituting for $\{u\}$ and $\{\tilde{u}\}$ from eqn. (12) and (13), and requiring that the resulting eqn. hold for all choices of $\{\tilde{\delta}\}$ we arrive at the following system of algebraic equations.

$$[K_{IJ}]\{\delta_J\} - \{F_I\} = 0, \tag{17}$$

where

$$\begin{aligned}[K_{IJ}] = &\int_{S_\alpha} \left([\tilde{B}_I]^T [D][B_J]\right) d\Omega \\ &- \int_{\Gamma_{\alpha u}} \left([\psi_I]^T [n][D][B_J]\right) d\Gamma \\ &- \int_{\Gamma_{\alpha 0}} \left([\psi_I]^T [n][D][B_J]\right) d\Gamma, \end{aligned} \tag{18}$$

$$\begin{aligned}\{F_I\} = &\int_{\Gamma_{\alpha q}} [\psi_I]^T \{\overline{q}\} d\Gamma \\ &+ \int_{S_\alpha} [\psi_I]^T \{\overline{f}_i\} dS \\ &+ L_i(\pm t/2) \int_{S_\alpha} [\psi_I]^T \{q^{\pm}\} d\Omega. \end{aligned} \tag{19}$$

Equations like (17) are found for each $S_\alpha$, $\alpha = 1,2,\ldots,M$. Essential boundary conditions, as described later in this section, are imposed and the equations are solved simultaneously for $\{\delta\}$.

### 3.2 Basis functions of the moving least squares approximation

We find basis functions $\{\phi_J\}$ by the moving least squares (MLS) approximation; see Lancaster and Salkauskas (1981) for details. For the sake of completeness, we briefly describe below the MLS approximation. The approximation $f^h(x,y)$ of a scalar-valued function $f(x,y)$ defined on $S_\alpha$ is written as

$$f^h(x,y) = \sum_{j=1}^{m} p_j(x,y)a_j(x,y), \tag{20}$$

where

$$\mathbf{p}^T(x,y) = \{1,x,y,x^2,xy,y^2,\ldots\}, \tag{21}$$

is a complete monomial in $(x,y)$ having $m$ terms. For complete monomials of degrees 1, 2 and 3, $m = 3$, 6 and 10 respectively. The unknown coefficients $a_1,a_2,\ldots,a_m$ are functions of $\mathbf{x} = (x,y)$, and are determined by minimizing $J$ defined by

$$J = \sum_{i=1}^{n} W(\mathbf{x}-\mathbf{x}_i)[\mathbf{p}^T(\mathbf{x}_i)\mathbf{a}(\mathbf{x}) - \hat{f}_i]^2, \tag{22}$$

where $\hat{f}_i$ is the ficticious value of $f$ at the point $(x_i,y_i)$, and $n$ is the number of points in the domain of influence of $\mathbf{x}$ for which the weight function $W(\mathbf{x}-\mathbf{x}_i) \neq 0$. We take

$$W(\mathbf{x}-\mathbf{x}_i) = \begin{cases} 1-6\left(\dfrac{d_i}{r_w}\right)^2+8\left(\dfrac{d_i}{r_w}\right)^3-3\left(\dfrac{d_i}{r_w}\right)^4, & 0 \le d_i \le r_w, \\ 0, & d_i \ge r_w, \end{cases} \tag{23}$$

where $d_i = |\mathbf{x}-\mathbf{x}_i|$ is the distance between points $\mathbf{x}$ and $\mathbf{x}_i$, and $r_w$ is the size of the support of the weight function $W$. Thus the support of $W$ is a circle of radius $r_w$ with center at the point $\mathbf{x}_i$.

The stationarity of $J$ with respect to $\mathbf{a}(\mathbf{x})$ gives the following system of linear equations for the determination of $\mathbf{a}(\mathbf{x})$:

$$\mathbf{A}(\mathbf{x})\mathbf{a}(\mathbf{x}) = \mathbf{B}(\mathbf{x})\hat{\mathbf{f}}, \tag{24}$$

where

$$\begin{aligned} \mathbf{A}(\mathbf{x}) &= \sum_{i=1}^{n} W(\mathbf{x}-\mathbf{x}_i)\mathbf{p}^T(\mathbf{x}_i)\mathbf{p}(\mathbf{x}_i), \\ \mathbf{B}(\mathbf{x}) &= [W(\mathbf{x}-\mathbf{x}_1)\mathbf{p}(\mathbf{x}_1),\ W(\mathbf{x}-\mathbf{x}_2)\mathbf{p}(\mathbf{x}_2), \\ &\quad \ldots, W(\mathbf{x}-\mathbf{x}_n)\mathbf{p}(\mathbf{x}_n)]. \end{aligned} \tag{25}$$

Substitution for $\mathbf{a}(\mathbf{x})$ from (24) into (20) gives

$$f^h(\mathbf{x}) = \sum_{j=1}^{m} \phi_j(\mathbf{x})\hat{f}_j, \tag{26}$$

where

$$\phi_k(\mathbf{x}) = \sum_{j=1}^{m} p_j(\mathbf{x})[\mathbf{A}^{-1}(\mathbf{x})\mathbf{B}(\mathbf{x})]_{jk}, \tag{27}$$

may be considered as the basis functions of the MLS approximation. It is clear that $\phi_k(x_j)$ need not equal the Kronecker delta $\delta_{kj}$. In order for the matrix $\mathbf{A}$, defined by $(25)_1$, to be invertible, the number $n$ of points in the domain of influence of $\mathbf{x}$ must at least equal $m$. For $m$ equal to 3 or 6, Chati and Mukherjee (2000) have found that $15 \le n \le 30$ gives acceptable results for two-dimensional elastostatic problems. For an elastodynamic problem, Batra and Ching (2002) used Gauss weight functions, the complete set of quadratic monomials and $r_w = 3.5$ times the distance to the third nearest node to the node at $\mathbf{x}_i$. Thus $r_w$ and the locations of nodes in $S_\alpha$ and hence $S$ must be such that $n$ satisfies the required constraint. We take

$$r_w = \rho h_i \tag{28}$$

where $h_i$ is the distance from node $i$ to its nearest neighbor, and $\rho$ is a scaling parameter.

### 3.3 MLPG1 and MLPG5 formulations

Atluri and Shen (2002a,b) classified the weak form (17) as MLPG1 and MLPG5 according as $\psi_J = W(\mathbf{x}-\mathbf{x}_J)$ or $\psi_J = H(\mathbf{x}-\mathbf{x}_J)$ where $H(\mathbf{x})$ is the Heaviside step function. Even though the derivative of a Heaviside step function is a delta function, the area integrals over $S_\alpha$ in eqn. (18) do not vanish identically in MLPG5 since expressions for $\eta_{i(3)}$, $\eta_{i(4)}$ and $\eta_{i(5)}$ involve terms with no derivatives. The MLPG5 formulation for the compatible HOSNDPT differs from the corresponding 2-dimensional elastostatic problem without body forces in which area integrals vanish identically. Note that

$K_{IJ} \neq K_{JI}$ in both MLPG1 and MLPG5, and $K_{IJ}$ need not be positive semidefinite.

The region $S_\alpha$ associated with node $\alpha$ is taken to be a circle of radius $h_\alpha$ with center at $\mathbf{x}_\alpha$. Integrals appearing in equations (18) and (19) are evaluated by using a Gauss quadrature rule. For each Gauss quadrature point $\mathbf{x}_Q$, the MLS basis functions are found and the integrand is evaluated at $\mathbf{x}_Q$. The number of Gauss points and the scaling parameter $\rho$ in eqn. (28) affect computed results; these will be elaborated upon in Section 4.

### *3.4 Imposition of essential boundary conditions*

We use the matrix transform technique (e.g. see Atluri and Shen (2002a)) to impose essential boundary conditions. Let $D$ and $I$ denote respectively the set of nodes where $x$-displacements are and are not prescribed; a similar treatment holds for $y$- and $z$-displacements. Writing the $x$-displacements of nodes as $\{u\}$, we have

$$\{u\} = \left\{ \begin{array}{c} u_D \\ u_I \end{array} \right\} = \left[ \begin{array}{cc} \phi_{DD} & \phi_{DI} \\ \phi_{ID} & \phi_{II} \end{array} \right] \left\{ \begin{array}{c} \delta_D \\ \delta_I \end{array} \right\}. \tag{29}$$

Solving the first of these equations for $\delta_D$, we get

$$\{\delta\} = \left\{ \begin{array}{c} \delta_D \\ \delta_I \end{array} \right\} = \left\{ \begin{array}{c} \phi_{DD}^{-1} u_D \\ 0 \end{array} \right\} + \left[ \begin{array}{c} -\phi_{DD}^{-1}\phi_{DI} \\ I \end{array} \right] \{\delta_I\}, \tag{30}$$

where 0 and $I$ are the null and the identity matrices respectively. Substitution from (30) into (17) and the premultiplication of the resulting equation by $\left\{ \begin{array}{c} -\psi_{DD}^{-1}\psi_{DI} \\ I \end{array} \right\}^T$ gives

$$[\overline{K}_{IJ}]\{\delta_I\} - \{\overline{F}_I\} = 0, \tag{31}$$

where

$$[\overline{K}_{IJ}] = \left[ \begin{array}{c} -\psi_{DD}^{-1}\psi_{DI} \\ I \end{array} \right]^T [K_{IJ}] \left[ \begin{array}{c} -\phi_{DD}^{-1}\phi_{DI} \\ I \end{array} \right], \tag{32}$$

$$\{\overline{F}_I\} = \left[ \begin{array}{c} -\psi_{DD}^{-1}\psi_{DI} \\ I \end{array} \right]^T \{F_I\} + \left[ \begin{array}{c} -\psi_{DD}^{-1}\psi_{DI} \\ I \end{array} \right] [K_{IJ}] \left\{ \begin{array}{c} \phi_{DD}^{-1} u_D \\ 0 \end{array} \right\}. \tag{33}$$

We note that once eqn. (31) has been solved for unknown degrees of freedom $\delta_I$, displacements of all nodes are known. $\eta_i$ at any point $\mathbf{x}$ can then be evaluated from (15), strains can be found from eqn. (6) and stresses can be determined by using eqn. (8).

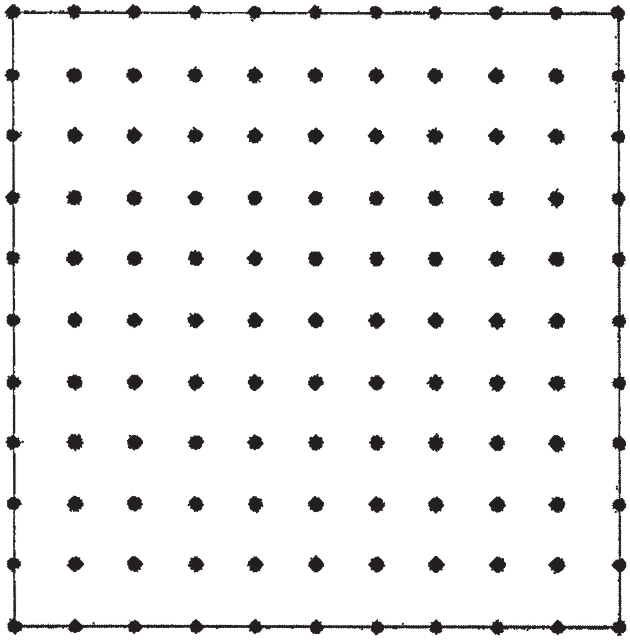

Figure 2: Locations of uniformly distributed nodes on the midsurface

## 4 Numerical Results

We compute results for a square plate made of a homogeneous and isotropic material and compare them with those available in the literature. We have set Poisson's ratio $= 0.3$, $\rho = 15$, $K = 6$, $M = 196$ and $m = 15$, i.e., complete monomials of degree 4 are considered in eqn. (21). Equal number of uniformly spaced nodes are placed in the $x$-and $y$-directions (cf. Fig. 2). The non-dimensional displacement $\overline{\mathbf{u}}$ is related to the dimensional displacement $\mathbf{u}$ by

$$\overline{\mathbf{u}} = \frac{100Et^3}{12q_0a^4(1-\nu^2)}\mathbf{u}, \tag{34}$$

where $E$ is Young's modulus, $q_0$ the uniformly distributed normal traction on the top surface of the plate, and $a$ is the length of a side of the square plate. The following boundary conditions are imposed at a simply supported $(S)$, a clamped $(C)$ and a free $(F)$ edge.

Table 1
Non-dimensional centroidal deflection of a thick square plate with $t/a = 0.2$

| | SSSS | SCSC | SFSF |
|---|---|---|---|
| MLPG1 | 0.4798 | 0.2928 | 1.4362 |
| MLPG5 | 0.4793 | 0.2928 | 1.4368 |
| Kant & Hinton (1980) | 0.4900 | 0.3016 | 1.4496 |
| Yuan & Miller (1992) | 0.4905 | 0.3021 | 1.4542 |
| Lee et al. (2002) | 0.4904 | 0.3021 | 1.4539 |
| Kant (1982) | 0.4800 | 0.2930 | 1.4304 |
| Kocak & Hassis (2002) | 0.4782 | 0.2920 | - |

Table 2
Non-dimensional deflection of the centroid of a square plate of different thicknesses

| t/a | SSSS | | | | | CCCC | | | |
|---|---|---|---|---|---|---|---|---|---|
| | MLPG1 | MLPG5 | Sinivas et al. (1969) | Kocak & Hassis (2002) | FEM | MLPG1 | MLPG5 | Srinivas & Rao (1973) | FEM |
| 0.1 | 0.4220 | 0.4275 | 0.4249 | 0.4200 | 0.4249 | 0.1468 | 0.1476 | 0.1496 | 0.1486 |
| 0.2 | 0.4798 | 0.4793 | - | 0.4786 | 0.4803 | 0.2112 | 0.2103 | 0.2134 | 0.2124 |
| 0.3 | 0.5717 | 0.5589 | - | - | 0.5710 | 0.3119 | 0.3064 | - | 0.3129 |
| 0.4 | 0.6967 | 0.6807 | - | - | 0.6952 | 0.4470 | 0.4408 | - | 0.4471 |
| 0.5 | 0.8511 | 0.8304 | - | - | 0.8487 | 0.6125 | 0.6050 | - | 0.6114 |

$$
\begin{aligned}
&S: \sigma_{xx} = 0,\ w = v = 0 \text{ on } x = 0, a;\\
&\quad \sigma_{yy} = 0,\ u = w = 0 \text{ on } y = 0, b;\\
&C: u = v = w = 0, x = 0, a;\ y = 0, b;\\
&F: \sigma_{xx} = \sigma_{xy} = \sigma_{xz} = 0 \text{ on } x = 0, a;\\
&\quad \sigma_{yy} = \sigma_{yx} = \sigma_{yz} = 0 \text{ on } y = 0, b. \qquad (35)
\end{aligned}
$$

Henceforth $S$ denotes a simply supported edge rather than the midsurface of the plate.

For a thick square plate with $a = 250$ mm and $t/a = 0.2$, Table 1 compares the presently computed centroidal deflection of the midsurface of the plate under different edge conditions with those obtained by other investigators. It is clear that both MLPG1 and MLPG5 solutions agree very well with those of other researchers. Present results differ slightly from those of Kant and Hinton (1980), Yuan and Miller (1992) and Lee et al. (2002) since they used a first-order shear deformation theory with a shear correction factor of $\sqrt{5/6}$; no such correction factor is used in the present compatible HOSNDPT. When two opposite edges are clamped and the other two edges are simply supported, the centroidal deflection is nearly 60% of that when all four edges are simply supported. However, when two opposite edges are free and the other two are simply supported, then the centroidal deflection is nearly 3 times that when all four edges are simply supported.

For a square plate, Table 2 compares the effect of the aspect ratio on the centroidal deflection with all edges either simply supported or clamped; FEM results were obtained with the commercial code IDEAS by using 20-node brick elements; the number of uniform elements in the $x$-, $y$- and $z$-directions equalled 40, 40 and 4 respectively. Both MLPG1 and MLPG5 formulations yield centroidal deflections of the midsurface that are very close to those obtained by other methods. Values, obtained by different methods, of the centroidal deflection of the midsurface and of the nondimensional stress $\sigma_{xx}(t/a)^2/q_0$ at the center of the top surface of either a simply supported or a clamped plate are compared in Table 3. Again, the MLPG1 and MLPG5 methods give results close to the analytical solutions of Srinivas et al. (1969). Stresses and stress resultants for plates with different edge condi-

Table 3
Nondimensional deflection of the centroid and the nondimensional stress $\sigma_{xx}$ at the center of the top surface of a simply supported square plate

| t/a | Non-dimensional deflection | | | | Non-dimensional stress | | | |
|---|---|---|---|---|---|---|---|---|
| | MLPG1 | MLPG5 | Srinivas et al. (1969) | Iyengar et al. (1974) | MLPG1 | MLPG5 | Srinivas et al. (1969) | Iyengar et al. (1974) |
| 0.10 | 0.4220 | 0.4275 | 0.4249 | 0.4248 | 0.2887 | 0.2920 | 0.2900 | 0.2898 |
| 0.14 | 0.4412 | 0.4418 | 0.4427 | 0.4427 | 0.2932 | 0.2889 | 0.2930 | 0.2922 |

Table 4
Non-dimensional stress $\sigma_{xx}$ at the center of the top surface of a thick square plate

| t/a | SSSS | | | CCCC | | |
|---|---|---|---|---|---|---|
| | MLPG1 | MLPG5 | FEM | MLPG1 | MLPG5 | FEM |
| 0.1 | 0.2887 | 0.2920 | 0.2900 | 0.1432 | 0.1450 | 0.1440 |
| 0.2 | 0.2984 | 0.3020 | 0.2976 | 0.1617 | 0.1589 | 0.1613 |
| 0.3 | 0.3129 | 0.3110 | 0.3099 | 0.1895 | 0.1836 | 0.1877 |
| 0.4 | 0.3333 | 0.3286 | 0.3283 | 0.2274 | 0.2224 | 0.2235 |
| 0.5 | 0.3640 | 0.3692 | 0.3568 | 0.2877 | 0.2725 | 0.2725 |

Table 5
Non-dimensional stress resultants for a SCSC thick plate

| Point (x/a,y/a) | Stress resultant | t/a=0.1 | | | | t/a=0.2 | | | |
|---|---|---|---|---|---|---|---|---|---|
| | | MLPG1 | MLPG5 | Kant & Hinton (1980) | Lee et al. (2002) | MLPG1 | MLPG5 | Kant & Hinton (1980) | Lee et al. (2002) |
| (0.5,0.5) | $M_{xx}$ | 0.0257 | 0.0251 | 0.0258 | 0.0258 | 0.0300 | 0.0298 | 0.0292 | 0.0292 |
| (0.5,0.5) | $M_{yy}$ | 0.0333 | 0.0325 | 0.0332 | 0.0333 | 0.0341 | 0.0335 | 0.0330 | 0.0331 |
| (0.5,0.0) | $M_{yy}$ | 0.0758 | 0.0726 | 0.0697 | 0.0680 | 0.0672 | 0.0641 | 0.0626 | 0.0627 |
| (1.0,0.0) | $Q_x$ | 0.250 | 0.255 | 0.243 | 0.243 | 0.258 | 0.259 | 0.251 | 0.251 |
| (0.5,0.0) | $Q_y$ | 0.4656 | 0.4884 | 0.5000 | 0.5000 | 0.4856 | 0.4820 | 0.4750 | 0.4750 |

Table 6
Non-dimensional stress resultants for a SFSF thick plate

| Point (x/a,y/a) | Stress resultant | t/a=0.1 | | | | t/a=0.2 | | | |
|---|---|---|---|---|---|---|---|---|---|
| | | MLPG1 | MPLG5 | Kant & Hinton (1980) | Lee et al. (2002) | MLPG1 | MLPG5 | Kant & Hinton (1980) | Lee et al. (2002) |
| (0.5,0.5) | $M_{xx}$ | 0.122 | 0.123 | 0.122 | 0.122 | 0.1228 | 0.1224 | 0.1230 | 0.1230 |
| (0.5,0.5) | $M_{yy}$ | 0.0261 | 0.0256 | 0.0256 | 0.0256 | 0.0245 | 0.0246 | 0.0237 | 0.0237 |
| (1.0,0.5) | $Q_x$ | 0.465 | 0.466 | 0.460 | 0.460 | 0.4600 | 0.4640 | 0.4560 | 0.4570 |

tions are compared in Tables 4, 5 and 6. In every case the MLPG1 and the MLPG5 techniques yield results very close to those obtained either by the FEM or by other researchers. Here

$$M_{xx} = \frac{1}{q_0 a^2}\int_{-t/2}^{t/2} z\sigma_{xx}dz,\ Q_x = \frac{1}{q_0 a}\int_{-t/2}^{t/2}\sigma_{xz}dz, \qquad (36)$$

etc.

We now delineate the effect of different parameters on the quality of the MLPG solutions.

### *4.1 Order of plate theory*

In order to delineate the acceptable order of the plate theory to use for a given plate, we have plotted in Figs. 3a-4b the nondimensional centroidal deflection and the nondimensional stress at the center of the top surface versus $K$ for a *CCCC* square plate with a uniformly distributed pressure applied on the top surface. For the MLPG1 and the MLPG5, $K = 3$ for $t/a \leq 0.1$ gives converged values of the deflection and the stress. However, for a plate with $t/a > 0.1$, one should use $K = 4$ for the MLPG1 and $K = 5$ for the MLPG5 formulations. The stress values computed with the MLPG5 exhibit oscillations of higher amplitude with an increase in the value of $K$ than those obtained from the MLPG1 method.

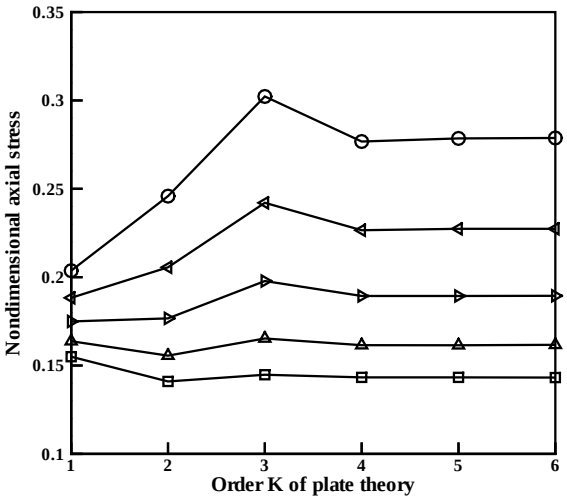


Figure 3b: Nondimensional stress $\sigma_{xx}$ vs. the order $K$ of the plate theory with the MLPG1 formulation. $t/a = 0.1$ $t/a = 0.2$ $t/a = 0.3$ $t/a = 0.4$ $t/a = 0.5$

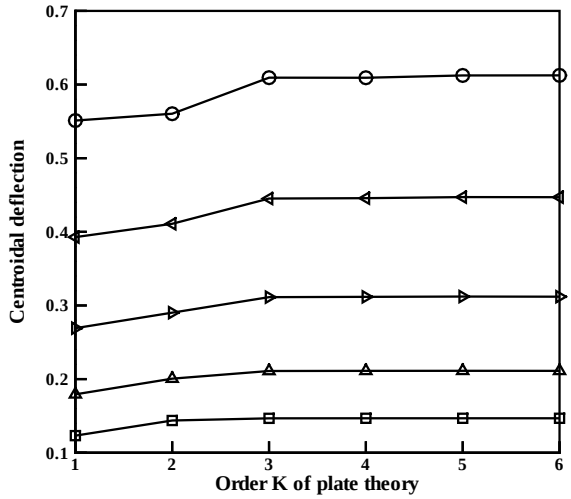


Figure 3a: Centroidal deflection vs. the order $K$ of the plate theory with the MLPG1 formulation. $t/a = 0.1$ $t/a = 0.2$ $t/a = 0.3$ $t/a = 0.4$ $t/a = 0.5$

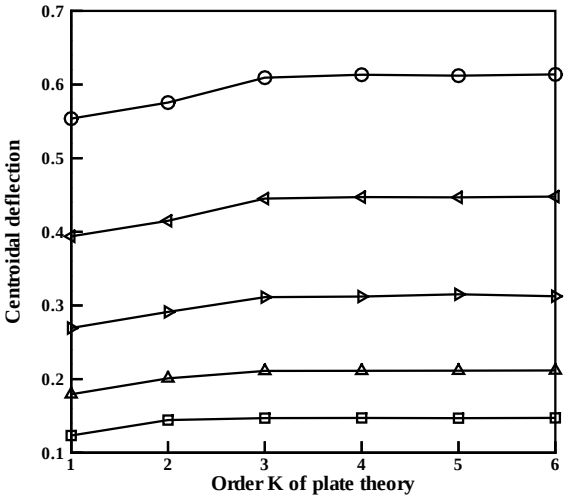


Figure 4a: Centroidal deflection vs. the order $K$ of the plate theory with the MLPG5 formulation. $t/a = 0.1$ $t/a = 0.2$ $t/a = 0.3$ $t/a = 0.4$ $t/a = 0.5$

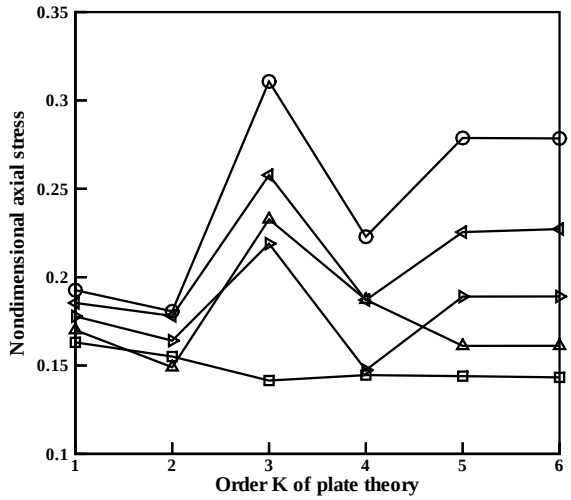


Figure 4b: Nondimensional stress $\sigma_{xx}$ vs. the order $K$ of the plate theory with the MLPG5 formulation. $t/a = 0.1$ $t/a = 0.2$ $t/a = 0.3$ $t/a = 0.4$ $t/a = 0.5$

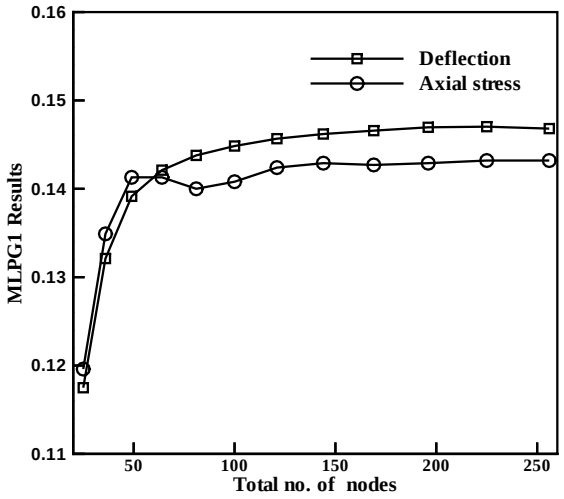


Figure 5: Convergence of the centroidal deflection and of the nondimensional axial stress $\sigma_{xx}$ at the center of the top surface of a square plate; results obtained with the MLPG1 formulation.

### *4.2 Number of nodes*

For a square plate we considered uniformly distributed nodes with the same number of nodes on each side for the two MLPG formulations; other variables were assigned the following values: $t/a = 0.1$, $K = 6$, $m = 15$, $\rho = 15$. Figures 5 and 6 exhibit the convergence of the centroidal deflection and the nondimensional stress at the top surface of a simply supported plate with uniform normal tractions applied on the top surface. Whereas the centroidal deflection computed with the two formulations converges monotonically, the stress does not. The amplitude of the oscillation in the axial stress value is higher for the MLPG5 formulation than that for the MLPG1 method. For both formulations, 13 uniformly spaced nodes on each side provide essentially converged results. Numerous case studies revealed that very good results for plates with $t/a > 0.1$ could not be obtained with less than 150 nodes even when the number of Gauss points used to numerically evaluate integrals in (18) and (19) was increased.

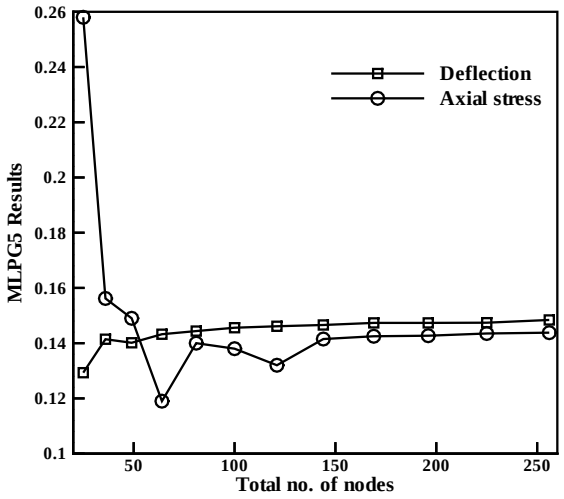


Figure 6: Convergence of the centroidal deflection and of the nondimensional axial stress $\sigma_{xx}$ at the center of the top surface of a square plate; results obtained with the MLPG5 formulation.

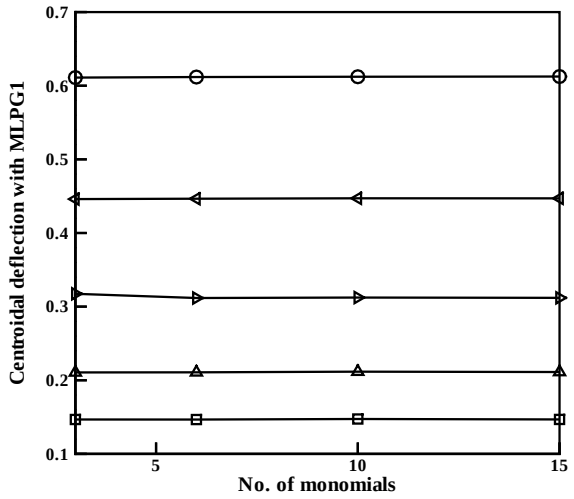


Figure 7a: Centroidal deflection vs. number of monomials in the MLS basis function. $t/a = 0.1$ $t/a = 0.2$ $t/a = 0.3$ $t/a = 0.4$ $t/a = 0.5$

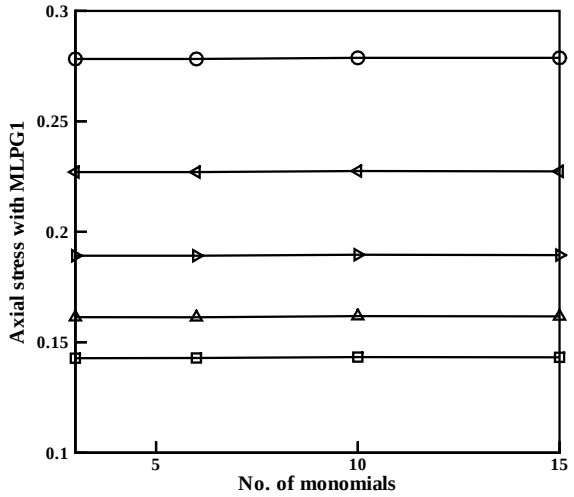


Figure 7b: Axial stress $\sigma_{xx}$ at the center of the top surface vs number of monomials in the MLS basis functions. $t/a = 0.1$ $t/a = 0.2$ $t/a = 0.3$ $t/a = 0.4$ $t/a = 0.5$

### *4.3 Number $m$ of monomials used to find MLS basis functions*

It seems intuitive that more terms in the expression (21) for **p** will lead to improved results. However, a larger value of $m$ will necessitate larger values of $\rho$ and of the number $N_Q$ of quadrature points. For $K = 6$, $\rho = 15$, $N_Q = 9 \times 9 = 81$, and number of nodes $= 256$, Figures 7a and 7b depict, for the MLPG1 formulation, the centroidal deflection and the axial stress at the center of the top surface of a clamped-clamped square plate; similar results were obtained with the MLPG5 method. It is clear that for all values of $t/a$ considered, $m = 6$ or a complete set of quadratic monomials gives good values of the two variables plotted in these Figs.

### *4.4 Effect of $\rho$*

The value of $\rho$ in eqn. (28) usually depends upon $m$, i.e., the number of monomial terms included in the expression for **p** in eqn. (21). For a given distribution of nodes, $\rho$ should be large enough so that the matrix **A** defined by eqn. $(25)_1$ is invertible. Chati and Mukherjee (2000) found that, for $m = 3$ or 6, a good value of $\rho$ should be such that 15 to 30 nodes lie in the region $|\mathbf{x} - \mathbf{x}_Q| \leq \rho h_Q$. For a thick square simply supported plate with $t/a = 0.2$, and $K = 6$, $m = 15$, $N_Q = 9 \times 9 = 81$, number of nodes $= 256$, Figs. 8 and 9 exhibit the dependence upon $\rho$ of the nondimensional centroidal deflection and of the axial stress at the center of the top surface for the MLPG1 and the MLPG5 formulations respectively. The centroidal deflection computed with the MLPG5 method has converged for $\rho = 9$ and that with the MLPG1 for $\rho = 12$. However, the convergence of the axial stress requires $\rho = 13$ for the MLPG5 and $\rho \geq 15$ for the MLPG1 formulations. Acceptable values of the deflection and the axial stress are obtained with $\rho = 8$ for the two formulations.

### *4.5 Effect of number of quadrature points*

We consider a clamped square plate and study the effect of varying the number $N_Q$ of quadrature points on the computed results.Figures 10 and 11 exhibit, for plates of different aspect ratios $t/a$, the dependence upon $N_Q$ of the computed centroidal deflection and of the axial stress at the center of the top surface of the plate. For $0.1 \leq \frac{t}{a} \leq 0.5$, the MLPG5 requires 64 quadrature points for computing good values of these two variables. However, the MLPG1 formulation needs 64 quadrature points for computing converged values of the centroidal deflection and of the axial stress for $t/a \geq 0.4$.

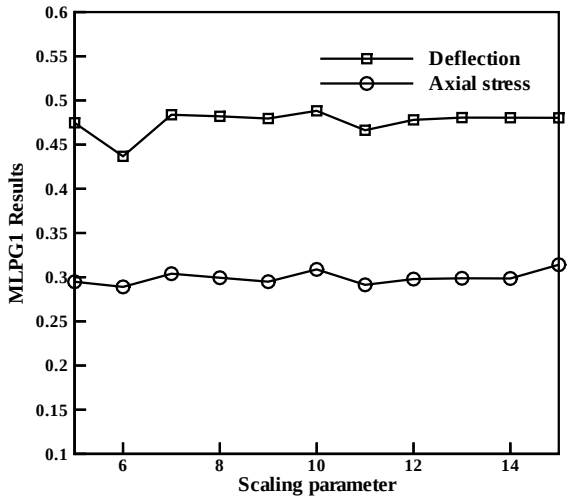


Figure 8: MLPG1 results vs. the scaling parameter. ρ.

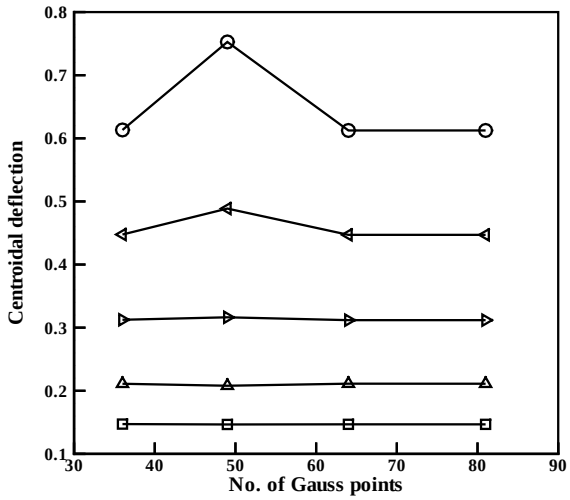


Figure 10a: MLPG1 results vs. number of Gauss points. $t/a = 0.1$ $t/a = 0.2$ $t/a = 0.3$ $t/a = 0.4$ $t/a = 0.5$

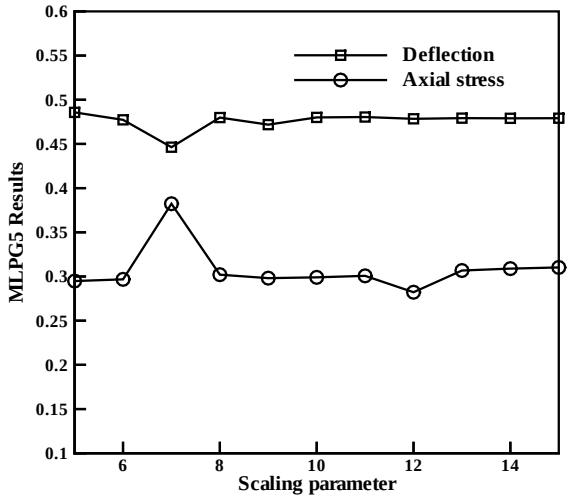


Figure 9: MLPG5 results vs. the scaling parameter, ρ.

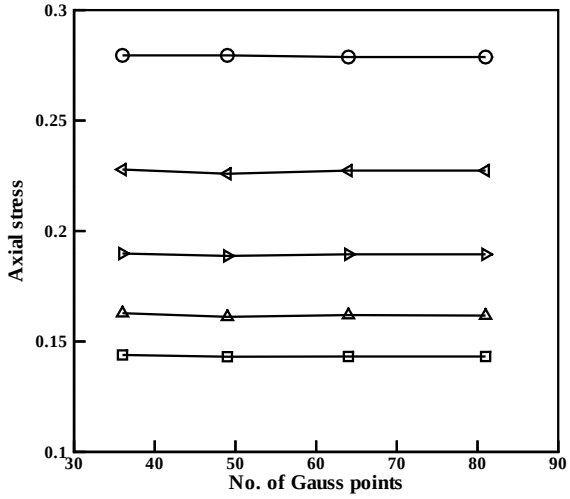


Figure 10b: MLPG1 results vs. number of Gauss points. $t/a = 0.1$ $t/a = 0.2$ $t/a = 0.3$ $t/a = 0.4$ $t/a = 0.5$

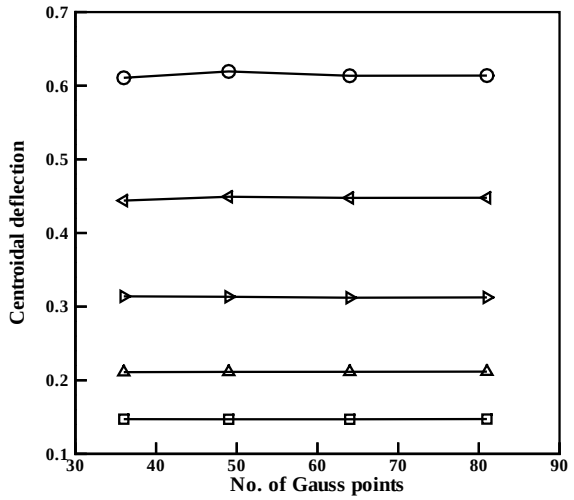


Figure 11a: MLPG5 results vs. number of Gauss points. $t/a = 0.1$ $t/a = 0.2$ $t/a = 0.3$ $t/a = 0.4$ $t/a = 0.5$

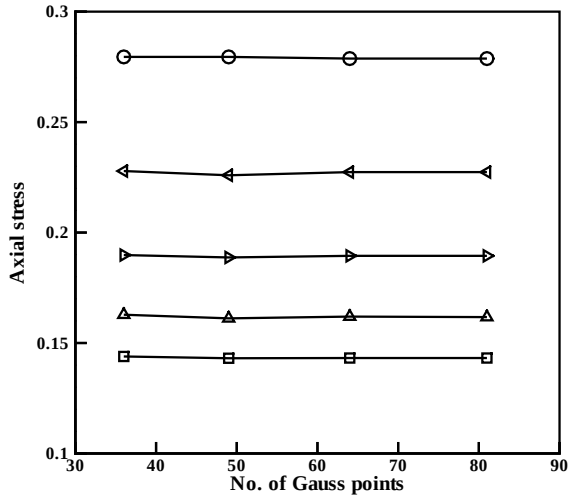


Figure 11b: MLPG5 results vs. number of Gauss points. $t/a = 0.1$ $t/a = 0.2$ $t/a = 0.3$ $t/a = 0.4$ $t/a = 0.5$

## 5 Conclusions

We have used two meshless local Petrov-Galerkin formulations, proposed by Atluri and Shen (2002a,b), namely the MLPG1 and the MLPG5, to find an approximate solution for deformation fields in a thick plate with edges subjected to different boundary conditions. Whereas in MLPG1 the test function is set equal to the weight function of the moving least squares approximation, in MLPG5 the test function equals a Heaviside step function. Deformations of the plate are modeled by a higher-order shear and normal deformable theory developed by Batra and Vidoli (2002). For the mechanical problem, a $K$th order plate theory has $3(K+1)$ unknowns at each point on the midsurface of the plate. Thus for a plate with all edges free and $M$ nodes on the midsurface, there will be $3(K+1)M$ unknowns and an equal number of linear algebraic equations will need to be solved simultaneously.

It is found that the MLPG1 and the MLPG5 formulations are very effective in analyzing elastostatic deformations of a plate. Computed values of the centroidal deflection and the normal stress at the center of the top surface match well with those either reported by other investigators or found from the 3-dimensional analysis of the problem by the finite element method. Convergence studies with respect to the number $M$ of uniformly distributed nodes, the number $N_Q$ of quadrature points used to evaluate integrals numerically, the order of complete monomials used to find basis functions of the moving least squares (MLS) approximation, the order of the plate theory, and the radius of the circular support of the weight function have been carried out. For $t/a \leq 0.1$, a 3rd-order plate theory is adequate and for $t/a > 0.1$ a 5th-order shear and normal deformable plate theory should be used. In general, values computed with the MLPG1 formulation converge monotonically to their "exact" values but those computed with the MLPG5 exhibit oscillations. Complete monomials of degree 2 are adequate in the polynomial basis functions employed in the MLS approximation. 169 uniformly spaced nodes are sufficient for obtaining essentially converged results. With no partitioning (see Atluri and Shen (2002a,b)) of the domain of integration, 64 quadrature points should be used to evaluate integrals appearing in the stiffness matrix and the load vector.

When essential boundary conditions are imposed by the penalty method, results for two-dimensional elastostatic problems have been found to be less sensitive to the value of the penalty parameter provided that it is greater than a critical value. For the plate problem studied herein, the value of the penalty parameter affected noticeably the computed results. This could be due to our attempt to sat-

isfy three-dimensional boundary conditions with a two-dimensional theory. Batra and Ching (2002) found that the time step used to compute a stable solution of a two-dimensional elastodynamic problem by the MLPG1 formulation and the explicit central-difference method also depends upon the value assigned to the penalty parameter.

**Acknowledgements:** This work was partially supported by the ONR grant N00014-98-1-0300 to Virginia Polytechnic Institute and State University with Dr. Y. D. S. Rajapakse as the congnizant program manager. L. F. Qian's work was also partially supported by the China Scholarship Council.

## References

**Atluri S.N. and Shen S.P.** (2002a): *The Meshless Local Petrov-Galerkin (MLPG) Method*. Tech Science Press.

**Atluri S.N. and Shen S.P.** (2002b): The Meshless Local Petrov-Galerkin (MLPG) Method: A Simple & Less-costly Alternative to the Finite Element and Boundary Element Methods. *CMES: Comp. Modeling in Eng'g. & Sci.*, Vol. 1, pp. 11-51.

**Atluri S.N. and Zhu T.**(2000): The Meshless Local Petrov-Galerkin (MLPG) Approach for Solving Problems in Elasto-statics. *Computational Mechanics*, Vol. 25, pp. 169-179.

**Atluri S.N., Kim H.G. and Cho J.Y.**(1999): A Critical Assessment of the Truly Meshless Local Petrov-Galerkin (MLPG) and Local Boundary Integral Equation (LBIE) Methods. *Computational Mechanics*, Vol. 24, pp. 348-372.

**Atluri S.N. and Zhu T.** (1998): A New Meshless Local Petrov-Galerkin (MLPG) Approach in Computational Mechanics. *Computational Mechanics*, Vol. 22, pp. 117-127.

**Batra R.C. and Ching H.K**(2002): Analysis of Elastodynamic Deformations near a Crack/Notch Tip by the Meshless Local Petrov-Galerkin (MLPG) Method. *CMES:Computer Modeling in Engineering & Sciences*, Vol. 3(6), 731-742.

**Batra R.C. and Vidoli S.**(2002): Higher-order Piezoelectric Plate Theory Derived from a Three-dimensional Variational Principle. *AIAA Journal*, Vol. 40, pp. 91-104.

**Batra R.C., Vidoli S. and Vestroni F.**(2002): Plane Wave Solutions and Modal Analysis in Higher Order Shear and Normal Deformable Plate Theories. *Journal of Sound and Vibration*, Vol. 257, pp. 63-88.

**Chati M.K. and Mukherjee S.**(2000): The Boundary Node Method for Three-dimensional Problems in Potential Theory. *Int. J. Num. Meth. Eng.*, Vol. 47, pp. 1523-1547.

**Ching H.K. and Batra R.C.**(2001): Determination of Crack Tip Fields in Linear Elastostatics by the Meshless Local Petrov-Galerkin (MLPG) Method. *CMES:Computer Modeling in Engineering & Sciences*, Vol. 2(2), pp. 273-289.

**Gu Y.T. and Liu G.R.**(2001): A Meshless Local Petrov-Galerkin (MLPG) Method for Free and Forced Vibration Analyses for Solids. *Computational Mechanics*, Vol. 27, pp. 188-198.

**Iyengar K.T., Chandrashekhara K. and Sebastian V.K.**(1974): On the Analysis of Thick Rectangular Plates. *Ingenieur Archiv.*, Vol. 43, pp. 317-339.

**Kant T. and Hinton E.**(1980): Numerical Analysis of Rectangular Mindlin Plates by Segmentation Method. Civil Engineering Department, Report:C/R365/80, University of Wales, Swansea.

**Kant T.** (1982): Numerical Analysis of Thick Plates. *Computer Methods in Applied Mechanics and Engineering*, Vol. 31, pp. 1-18.

**Kocak S. and Hassis H.**(2002): A Higher Order Shear Deformable Finite Element for Homogeneous Plates. *Engineering Structures*, (in press).

**Lancaster P. and Salkauskas K.**(1981): Surfaces Generated by Moving Least Squares Methods. *Meth. Comput.*, Vol. 37, pp. 141-158.

**Lee K.H., Lim G.T. and Wang C.M.** (2002): Thick Levy Plate Re-visited. *International Journal of Solids and Structures*, Vol. 39, pp. 127-144.

**Lin H. and Atluri S.N.**(2000): Meshless Local Petrov-Galerkin (MLPG) Method for Convection-diffusion Problems. *CMES:Computer Modeling in Engineering & Sciences*, Vol. 1(2), pp. 45-60.

**Long S. and Atluri S.N.**(2002): A Meshless Local Petrov-Galerkin Method for Solving the Bending Problem of a Thin Plate. *CMES:Computer Modeling in Engineering & Sciences*, Vol. 3(1), pp. 53-64.

**Mindlin R.C., Medick M.A.**(1959): Extensional Vibrations of Elastic Plates. *Journal of Applied Mechanics*, Vol. 26, pp. 145-151.

**Srinivas S., Rao A.K. and Rao C.V.**(1969): Flexure of Simply Supported Thick Homogeneous and Laminated Rectangular Plates. *ZAMM*, Vol. 49, pp. 449-458.

**Srinivas S., Rao C.V. and Rao A.K.**(1970): An Exact Analysis for Vibration of Simply Supported Homogeneous and Laminated Thick Rectangular Plates. *Journal of Sound and Vibration*, Vol. 12, pp. 187-199.

**Srinivas S. and Rao A.K.**(1973): Flexure of Thick Rectangular Plates. *J. Appl. Mech.*, Vol. 39, pp. 298-299.

**Vidoli S. and Batra R.C.**(2000): Derivation of Plate and Rod Equations for a Piezoelectric Body from a Mixed Three-dimensional Variational Principle. *J. Elasticity*, Vol. 59, pp. 23-50.

**Warlock A., Ching H.K., Kapila A.K. and Batra R.C.**(2002): Plane Strain Deformations of an Elastic Material Compressed in a Rough Rectangular Cavity. *International Journal of Engineering Science*, Vol. 40, pp. 991-1010.

**Yang J.S. and Batra R.C.**(1995): Mixed Variational Principles in Nonlinear Piezoelectricity. *International Journal of Nonlinear Mechanics*. Vol.30, pp. 719-726.

**Yuan F.G. and Miller R.E.**(1992): Improved Rectangular Element for Shear Deformable Plates. *Journal of Engineering Mechanics, ASCE*, Vol. 118, pp. 312-328.